



Time-dependent CFD and quasi-static analysis of magnetorheological fluid dampers with experimental validation

Zekeriya Parlak*, Tahsin Engin

Department of Mechanical Engineering, Sakarya University, 54187 Sakarya, Turkey

ARTICLE INFO

Article history:

Received 20 June 2011

Accepted 13 August 2012

Available online 23 August 2012

Keywords:

Magnetorheological fluid

MR damper

MR fluid

Finite element

Computational fluid dynamics

CFD

ABSTRACT

Magnetorheological (MR) dampers can be controlled effectively by a magnetic field and with minimum power requirement. Under the magnetic field, MR fluid behaves as a non-Newtonian fluid with controllable viscosity. Damper performance can be enhanced by getting to know better the non-Newtonian flow in the annular gap of piston head.

In the study the non-Newtonian flow in the annular gap is investigated by a quasi-static analysis that enables to calculate plug thickness and damper force. Also CFD analysis of the MR damper is performed by using transient and deformed mesh to be able to simulate moving of piston head in the damper considering non-Newtonian regions. Results of the analyses have been compared to experimental data obtained from MR dampers manufactured for the study. Good agreement has been observed between experimental and analyses data. In addition, effects of stroke and velocity on the damper performance are examined in the study.

© 2012 Elsevier Ltd. All rights reserved.

1. Introduction

Magnetorheological (MR) fluid devices have been employed in many applications, especially transportation vehicle, building suspensions and biomedical, owing to their unique advantages. Magnetorheological fluid exhibits significant change in rheological properties under magnetic field. When a magnetic field is applied to the fluid, particles in the fluid form chains, and the suspension becomes like a semi-solid material in a few millisecond. Under the magnetic field, an MR fluid behaves as a non-Newtonian fluid with controllable viscosity. However, if the magnetic field is removed, the suspension turns to a Newtonian fluid and the transition between these two phases is highly reversible, which provides unique feature of magnetic-field controllability of the flow of MR fluids. If possible, an ability to obtain the flow phenomenon inside the MR damper can simplify assessments of the damper performance, thus it can be particularly useful in reducing the number of testing of prototypes and providing a good insight in the phenomena occurring in the MR damper. For that purpose, numerous analytical, experimental and numerical studies have been performed so far.

Wereley and Pang [1] developed a quasi-static model based on Bingham plastic model that can be characterized the damper performance using control ratio depending on nondimensional numbers. Felt et al. [2] and Dimock et al. [3] observed that Bingham

plastic model is inadequate to describe the shear-thinning flow in MR fluid. Hesselbach and Abel-Keilhack [4] implemented flow analysis of an active hydrostatic bearing with magnetorheological fluid using Bingham, Herschel–Bulkley and Bi-Bingham models. Wang [5] carried out flow analysis of MR fluid device using the Herschel–Bulkley model. Wang and Gordaninejad [6] improved a model to calculate pressure through pipes and parallel plates. Yasrebi et al. [7] presented electromagnetic and flow finite element analysis of a MR damper using ANSYS codes. Widjaja et al. [8] developed a mathematical model based on the Herschel–Bulkley model to describe flow characteristic that cannot be obtained as experimentally. Ericksen and Gordaninejad [9] presented a theoretical fluid mechanics-based model to predict the controllable damping force in terms of the physical parameters of the device, the magnetorheological fluid properties, the electromagnetic circuit parameters, and the input motion for semi-active suspension systems of off-road motorcycle. Attia and Ahmed [10] investigated the unsteady flow of a dusty viscous incompressible electrically conducting Bingham fluid through a circular pipe. Li and Du [11] investigated yield stress of a MR brake system experimentally based on Bingham Plastic model. Bullough et al. [12] implemented CFD analysis of a piezo-hydraulic valve using a user-defined subroutine in Fluent software that allows Bingham CFD model. Ellam et al. [13] investigated two-dimensional steady isothermal flows of a Bingham plastic between two plates, one of them moving and the other stationary and they used a CFD package to verify for similar flows. Susan-Resiga [14] presented blending rheological model that allows the identification of a yield point and that can be used in regular CFD

* Corresponding author. Tel.: +90 2642955495; fax: +90 2643460080.
E-mail address: zparlak@sakarya.edu.tr (Z. Parlak).

codes to compute the MR fluid flow. Lekic and Kok [15] implemented a CFD model using a moving mesh for the compressor with piston. Bompos and Nikolakopoulos [16] presented a simulation study via CFD and FEM for MR fluid journal bearing.

The present study deals with quasi-static analysis of fluid flow in the annular gap and CFD analysis of the MR damper. The quasi-static analysis is presented based on Navier–Stokes equations using Bingham plastic model for non-Newtonian region in the annular gap of piston head. Some assumptions are made to simplify the continuity and the Navier–Stokes equations, thus a nonlinear equation system is obtained as a function of location of plug thickness, which occurs as a result of non-Newtonian flow, in the annular gap. Pressure drop and damper force are calculated after solving of the nonlinear equation system. In addition, plug thicknesses obtained by quasi-static analysis are compared to the model presented by Wereley and Pang [1], which depends to dimensional Bi number, and an analytical presented firstly in the study. A CFD model is presented by using a commercial CFD package, ANSYS CFX 12.1, for the MR damper as three dimensional. The CFD analysis that is to implement with deformed (moving) mesh approach by taking into consideration movement of the piston has not been seen in the literature until the study, thus filling the gap in the literature. Flow magnitudes are observed and obtained their values of during piston movement due to moving mesh. Also, the CFD analysis that is with non-Newtonian flow modeled by Bingham CFD model is taken into consideration together with deformed mesh firstly in the study. The damper configurations performed by the quasi-static and CFD analyses are manufactured and tested. The test data are compared with both quasi-static and CFD analysis ones. In addition the dampers are tested to find out effect of stroke and velocity on the damper performance.

2. Quasi-static analysis of flow in MR damper

Flow inside the annular gap that behaves as non-Newtonian can be analyzed based on Navier–Stokes equations by using the Bingham plastic model. In the analysis, pressure drop along the gap can be obtained as function of MR fluid properties, geometry and volume flow rate. Cross-section of MR damper can be seen in Fig. 1.

Behavior of MR Fluid when active in other words under magnetic field in the gap, the fluid acts like a rigid body at below dynamic yield stress then fluid flow can be modeled considering the Bingham plastic model or the Herschel–Bulkley model. This plug region is called as pre-yield. In the pre-yield region, the local shear stresses have not yet exceeded the dynamic yield stress. When the local shear stresses exceed the dynamic yield stress, these regions are called as post-yield region, then the fluid acts like a viscous fluid.. The pre- and post-yield regions are shown in Fig. 2 with the velocity profile. As shown in Fig. 2, the velocity profile is divided into three regions: Regions I and III denote the post-yield regions and Region II denotes the pre-yield region [17]. As can be seen in Fig. 2, because there is no velocity gradient on the plug region, MR fluid flows as a rigid body.

The flow is occurred in an annular gap and with a constant piston velocity. Following assumptions are made to simplify the continuity and the Navier–Stokes equations in cylindrical coordinates.

Assumptions:

1. The flow is only in the z-direction, implying that $u_r=0$ and all partial derivatives with respect to r ($\partial/\partial r$) are zero.
2. The flow is steady in the annular gap implying that all partial derivatives with respect to t ($\partial/\partial t$) are zero.
3. The flow is incompressible implying that $\rho=\text{constant}$.

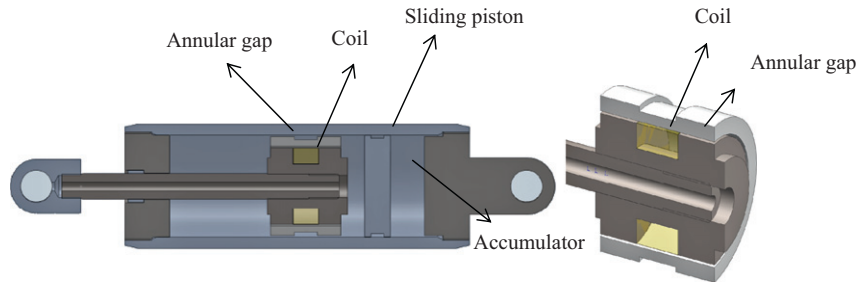


Fig. 1. Cross-section of MR damper.

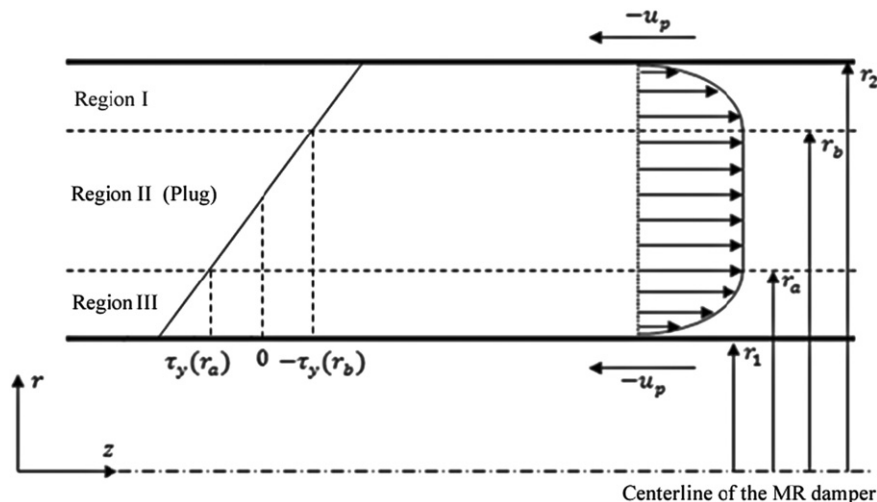


Fig. 2. Velocity and stress profiles across annular gap.

4. The flow is two dimensional and no swirl, implying $u_\theta=0$ and all partial derivatives with respect to θ ($\partial/\partial\theta$) are zero.
5. The flow is laminar and fully developed.
6. Gravitational effects are neglected.
7. A constant pressure gradient, (dP/dz) is applied in the z-direction.

Simplifying the continuity equation with respect to above assumptions yields

$$\frac{\partial u_z}{\partial z} = 0 \quad (1)$$

It does mean that u_z is not dependent on z then velocity stays constant at any location of z , it can be specified as $u_z=u=u(r)$.

z-momentum equation,

$$\frac{1}{\mu} \frac{\partial p}{\partial z} = \frac{1}{r} \frac{d}{dr} \left(r \frac{du}{dr} \right) \quad (2)$$

and r-momentum equation,

$$\frac{\partial p}{\partial r} = 0, \quad P = P(z) \quad (3)$$

as can be seen in Eq. (3) pressure is only dependent on z .

Shear stress is $\tau_{rz} = \mu(du/dr)$ and Eq. (2) can be rearranged as

$$r \frac{dP}{dz} = \frac{d(r\tau_{rz})}{dr} \quad (4)$$

when integrating Eq. (4) with respect to r shear stress can be obtained as follows:

$$\tau_{rz} = \frac{1}{2} \frac{dP}{dz} r + \frac{c_1}{r} \quad (5)$$

where c_1 is the integral constant.

The Bingham plastic model is used in the study in order to describe non-Newtonian behaviors of the MR fluid [1,3,18–21]

Bingham plastic model

$$\tau = \tau_y(B) \text{sgn}(\dot{\gamma}) + \mu_p \dot{\gamma} \quad |\tau| > |\tau_y|$$

$$\dot{\gamma} = 0 \quad |\tau| < |\tau_y| \quad (6)$$

where τ is shear stress, $\dot{\gamma}(du/dr)$ is shear rate, $\tau_y(B)$ is yield stress changing with magnetic flux intensity, and μ_p is plastic viscosity independent of magnetic field. Each region in Fig. 2 should be evaluated separately due to their different structures.

For plug region (II)

$$\begin{aligned} \tau_{rz}(r_a) &= \tau_y \\ \tau_{rz}(r_b) &= -\tau_y \end{aligned} \quad (7)$$

substituting Eq. (7) into Eq. (5) gives

$$\begin{aligned} \tau_y &= \frac{1}{2} \frac{dP}{dz} r_a + \frac{c_1}{r_a} \\ -\tau_y &= \frac{1}{2} \frac{dP}{dz} r_b + \frac{c_1}{r_b} \end{aligned} \quad (8)$$

when subtraction and summation are made, respectively, in Eq. (8) yields

$$c_1 = -\frac{1}{2} \frac{dP}{dz} r_a r_b \quad (9)$$

$$r_b - r_a = -\frac{2\tau_y}{dP/dz} \quad (10)$$

For post-yield region (III)

Since flows is nonlinear in the region III ($du/dr > 0$ and thus $\text{sgn}(du/dr)=1$), substituting Eq. (6) into Eq. (5) gives

$$\tau_y + \mu \frac{du}{dr} = \frac{1}{2} \frac{dP}{dz} r + \frac{c_1}{r} \quad (11)$$

integrating with respect to r

$$u(r) = \left(\frac{1}{4\mu} \frac{dP}{dz} r^2 + \frac{c_1}{\mu} \ln(r) - \frac{\tau_y}{\mu} r + c_2 \right) \quad (12)$$

c_2 is the integral constant which can be determined by the boundary conditions that is $r=r_1$ for $u=-u_p$

$$c_2 = -u_p - \frac{1}{4\mu} \frac{dP}{dz} r_1^2 - \frac{c_1}{\mu} \ln(r_1) + \frac{\tau_y}{\mu} r_1 \quad (13)$$

at that $u(r)$ concludes with

$$u(r) = \left(\frac{1}{4\mu} \frac{dP}{dz} (r^2 - r_1^2) + \frac{c_1}{\mu} \ln\left(\frac{r}{r_1}\right) - \frac{\tau_y}{\mu} (r - r_1) - u_p \right) r_1 \leq r \leq r_a \quad (14)$$

For post-yield region (I)

Since flow is nonlinear in the region I ($du/dr < 0$ and thus $\text{sgn}(du/dr)=-1$), substituting Eq. (6) into Eq. (5) gives

$$-\tau_y + \mu \frac{du}{dr} = \frac{1}{2} \frac{dP}{dz} r + \frac{c_1}{r} \quad (15)$$

$$u(r) = \left(\frac{1}{4\mu} \frac{dP}{dz} r^2 + \frac{c_1}{\mu} \ln(r) + \frac{\tau_y}{\mu} r + c_3 \right) \quad (16)$$

c_3 is the integral constant which can be determined by the boundary conditions that is $r=r_2$ for $u=-u_p$

$$c_3 = -u_p - \frac{1}{4\mu} \frac{dP}{dz} r_2^2 - \frac{c_1}{\mu} \ln(r_2) - \frac{\tau_y}{\mu} r_2 \quad (17)$$

at that $u(r)$ concludes with

$$u(r) = \left(\frac{1}{4\mu} \frac{dP}{dz} (r^2 - r_2^2) + \frac{c_1}{\mu} \ln\left(\frac{r}{r_2}\right) + \frac{\tau_y}{\mu} (r - r_2) - u_p \right) r_b \leq r \leq r_2 \quad (18)$$

It can be seen in Fig. 2 that $u(r_a)$ equals to $u(r_b)$ due to $du/dr=0$. Thus, when equalized to Eqs. (14) and (18) under the boundary conditions, pressure gradient can be obtained as follows:

$$\frac{dp}{dz} = \frac{4}{r_2^2 - r_1^2 + r_a^2 - r_b^2} \left[c_1 \ln\left(\frac{r_b r_1}{r_a r_2}\right) + \tau_y (r_b + r_a - r_1 - r_2) \right] \quad (19)$$

Total volume flow rate through the annular gap can be calculated by velocity profiles of these three regions in the gap, which yields

$$Q = 2\pi \int_{r_1}^{r_2} u(r) r dr \quad (20)$$

The velocity profiles in each of these three regions have been already known with equations above, then the total volume flow rate can be described by

$$\begin{aligned} Q &= \frac{\Pi}{24\mu} \left(12r_1^2 c_1 + 3r_1^4 \frac{dp}{dz} + 24r_1^2 u_p \mu - 8r_1^3 \tau_y + 3 \frac{dp}{dz} r_a^4 \right. \\ &\quad - 6 \frac{dp}{dz} r_1^2 r_a^2 + 24c_1 r_a^2 \ln\left(\frac{r_a}{r_1}\right) - 12c_1 r_a^2 - 16\tau_y r_a^3 \\ &\quad + 24r_a^2 \tau_y r_1 + 3 \frac{dp}{dz} r_b^4 + 12c_1 r_b^2 + 8\tau_y r_b^3 - 12r_2^2 c_1 \\ &\quad - 3r_2^4 \frac{dp}{dz} - 24r_2^2 u_p \mu - 8r_2^3 \tau_y - 6 \frac{dp}{dz} r_b^2 r_2^2 \\ &\quad \left. + 6 \frac{dp}{dz} r_2^2 r_a^2 - 24c_1 r_a^2 \ln\left(\frac{r_b}{r_2}\right) - 24\tau_y r_b r_a^2 + 24r_a^2 \tau_y r_2 \right) \end{aligned} \quad (21)$$

On the other hand, the total volume flow rate must be equal to volume flow rate displaced by the piston head as follows:

$$Q_I + Q_{II} + Q_{III} = Q_p = (A_p - A_r) u_p \quad (22)$$

where A_p is cross-sectional area of the piston head, and A_r is cross-sectional area of the piston rod.

Two equations are required in order to find the two unknowns, r_a and r_b . First equation can be obtained by equaling of Eqs. (21)

and (22)

$$Fonc_1 = Q - Q_p = 0 \quad (23)$$

Pressure gradient across the annular gap can be got by Eq. (10) as follows:

$$\frac{dP}{dz} = -\frac{2\tau_y}{r_b - r_a} \quad (24)$$

Second equation can be obtained by equaling of Eqs. (19) and (24). Thus, we have

$$Fonc_2 = \frac{4}{r_2^2 - r_1^2 + r_a^2 - r_b^2} \left[c_1 \ln \left(\frac{r_b r_1}{r_a r_2} \right) + \tau_y (r_b + r_a - r_1 - r_2) \right] + \frac{2\tau_y}{r_b - r_a} \quad (25)$$

The nonlinear system of the two equations, Eqs. (23) and (25), can be solved by determining values of r_a and r_b . Once the values are put into Eq. (24), pressure gradient can be obtained. Thus, pressure drop across active length in the annular gap is

$$\Delta P_{2t_k} = P_{t_k} - P_0 = -\frac{dP}{dz} 2t_k \quad (26)$$

where t_k is active length, the pressure drop caused by field-dependent yield stress is called as controllable or yield pressure drop. However, in inactive regions of the annular gap in which particularly adjacent to the coil winding, $(L - 2t_k)$, MR fluid exhibits a Newtonian like behavior and thus pressure drop should be evaluated separately. There is only viscous pressure drop in the region, Nguyen et al. [19] suggest the viscous pressure drop equation for annular gap is as follows:

$$\Delta P_{L-2t_k} = \frac{6\mu(L-2t_k)}{\pi R_1 g^3} Q \quad (27)$$

L is the annular gap length and R_1 is the average radius of the annular gap given by $R_1 = R - (g_n + 0.5g)$. Total pressure drop through the annular gap is

$$\Delta P_L = \Delta P_{2t_k} + \Delta P_{L-2t_k} = -\frac{dP}{dz} 2t + \frac{6\mu(L-2t_k)}{\pi R_1 g^3} Q \quad (28)$$

On the other hand, the total pressure drop can be calculated as follows [20]:

$$\Delta P_L = \Delta P_\mu + \Delta P_\tau = \frac{6Q\mu L}{\pi R_1 g^3} + c \frac{2t_k}{g} \tau_y \quad (29)$$

where ΔP_μ and ΔP_τ are the viscous and controllable pressure drop of MR damper, respectively. c is the coefficient which depends on the flow velocity, Spencer et al. [22] proposed the following approximate relation for the coefficient c :

$$c = 2.07 + \frac{6Q\mu}{6Q\mu + 0.4\pi R_1 g^2 \tau_y} \quad (30)$$

The damping force can be determined from

$$F_{rebound} = \Delta P_L (A_p - A_r) + F_s \quad (31)$$

$$F_{compression} = \Delta P_L A_p + F_s \quad (32)$$

where F_s is the friction force and measured experimentally.

Wereley and Pang [1] presented a method in order to calculate the plug region thickness. They suggested a cubic Eq. (33) in terms of nondimensional plug region thickness and nondimensional Bi number.

$$\frac{1}{2} \bar{\delta}^3 - \left[\frac{3}{2} + \frac{6}{Bi} \right] \bar{\delta} + 1 = 0, \quad 0 \leq \bar{\delta} \leq 1 \quad (33)$$

where $\bar{\delta}$ is nondimensional plug region thickness and Bi is nondimensional Bingham number; they can be determined from

$$\bar{\delta} = \frac{\delta}{g} = \frac{(r_b - r_a)}{g} \quad (34)$$

$$Bi = \frac{\tau_y}{\mu(u_0/g)} \quad (35)$$

where u_0 equals to $A_p/A_g u_p$.

The Bingham number is the ratio of the dynamic yield stress of a Bingham plastic material to the shear stress. The Bingham number is large when the damper shaft velocity is small, or when the damper is operating close to the yield point of the Bingham plastic material. The Bingham number is small when the damper shaft velocity is large, or when the damper is operating in a strongly post-yield condition. Also, the Bingham number is zero when the dynamic yield stress is zero, as is nearly the case in the absence of field. Thus, the Bingham number can be interpreted as a measure of how close the damper is operating to the yield condition [1].

3. Experimental study

3.1. Manufacturing of MR dampers

Three MR dampers are fabricated and tested to validate results of quasi-static and CFD analysis result for the study. Some dimensional are specified as constant for each damper as can be seen in Table 1. On the one hand, gap width, active pole (active) length and coil height are manufactured in different values (see Table 2). When active length is specified at different values, it is yielded at different values of coil height, then at different number of turn of the coils. In Table 2 can be seen number of turn, coil wire diameter values used and values of yield stress calculated by ANSYS Magnetostatic tool.

During the assembling, about 50 mm³ of MR fluid is filled without any air space in the cylinder volume obtained when sliding piston is kept at maximum stroke, then about 20 bar nitrogen gas is compressed in the accumulator. The dampers can be seen in Fig. 3 after the assembling.

3.2. Test set-up

The fabricated dampers were tested on a mechanical scotch-yoke type shock machine Roehrig MK-2150. The shock machine has its own software (SHOCK 6.3) to collect data from the data card. Its characteristic data curves are force vs. time, force vs. velocity, and force vs. displacement. The machine has also an IR

Table 1
MR damper constant dimensions.

Gap length	22 mm
Piston rod diameter	8 mm
Piston core diameter	14 mm
Coil width	4.9 mm
Inner diameter of cylinder	32 mm
Sliding piston width	8 mm
Inner length of cylinder	80 mm

Table 2
Gap width, active pole length, coil width and height.

Damp. no.	g (mm)	t (mm)	dk (mm)	NC	τ_y (Pa)
1	0.6	5	0.45	220	32.02
2	0.6	6	0.4	233	28.34
3	0.6	7	0.35	241	24.83

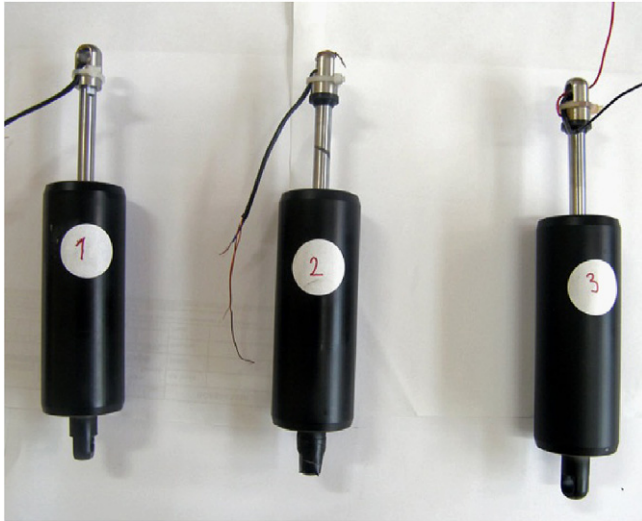


Fig. 3. Manufactured dampers.

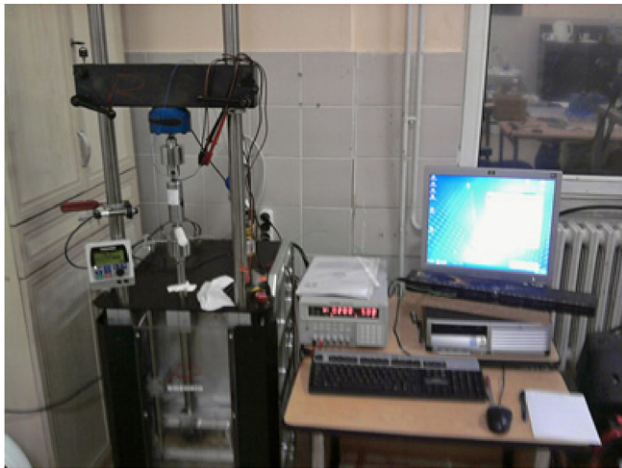


Fig. 4. Test machine with the damper under test.

temperature sensor to read the temperature data during the tests. Experimental set-up is shown in Fig. 4 with its main components. A programmable “GWinstek PPE 3223” power supply was used to feed current to coil of the MR damper.

The dynamic tests of the dampers is performed by varying applied current from 0 A to 2 A in increments of 0.25 A, while maintaining the piston velocity and stroke at constant levels of 0.05 m/s, 0.1 m/s, 0.15 m/s and 0.2 m/s and 5 mm and 25 mm, respectively. Force vs. time, force vs. displacement, and force vs. velocity curves are obtained and in addition temperature, gas force, friction force is measured for each test.

4. CFD analysis of MR dampers

CFD analysis was carried out CFX tool of ANSYS v.12.1 in the study. For computational time reduction, and assuming the fluid flow to be axi-symmetric, the dampers were modeled as a 45° slice of this computational domain. CFD analysis was realized on a moving (deformed) mesh that implies to a transient model.

Movement of the piston inside the cylinder can be simulated just by using the moving mesh. Moreover, damper force–velocity and damper force–displacement curves can be obtained by the transient analysis so that compared to experimental data. Regions not magnetized (Newton fluid) within the gap in parallel to coil and the regions that do magnetized (non-Newtonian fluid) within the gap in parallel to active (flange) length can be defined by CCL – CFX Command Language – expressions depending on time in the same computational domain. While moving the piston in the domain, it can be specified with the CCL expressions whether a node is in the active region or not.

According to varying damper dimensions, computational domain consists of about 6200 nodes and 25,000 tetrahedral volume elements. The mesh and boundaries can be seen in Fig. 5. Moving parts of the damper that are piston and sliding piston were taken into account while creating the mesh.

CFX v12.1 consists of CFX-Pre, which provides to able to specified boundary condition, flow type, fluid type and solution method, CFX-Solver, which solves equations of flow model by numerical methods considering convergence criteria specified on CFX-Pre, and CFX-Post, which gives numeric and visual results.

Non-Newtonian regions in the gap were defined in terms of viscosity by characterizing the material properties on CFX-Pre. The viscosity is expressed as a variable on CFX-Pre by using the Bingham CFD model [12] based on the Bingham plastic model. Bingham viscosity, μ_B , is defined in the Bingham CFD model as follows:

$$\begin{aligned} \mu_B &= \frac{\tau_{y,k}}{\dot{\gamma}} + \mu_p \quad \dot{\gamma} \geq \dot{\gamma}_k \\ \mu_B &= \mu_s \quad \dot{\gamma} < \dot{\gamma}_k \end{aligned} \quad (36)$$

In Fig. 6, $\tau_{y,k}$ is yield stress that defines transition to non-Newtonian region. μ_p is plastic viscosity, μ_s is high (solid-type) viscosity, $\dot{\gamma}_k$ is critical shear rate and is start point of transition to non-Newtonian from Newtonian.

In pre-yield region MR fluid has high viscosity (μ_s) for the Bingham plastic model. After the critical shear rate or critical yield stress is exceeded, viscosity decreases to value of the plastic viscosity (see Fig. 6). μ_B approaches infinity at low shear rates. To avoid problems due to the high viscosity, it should be defined that μ_s is 100–1000 times bigger than the plastic viscosity μ_p , then a high degree of computational precision is achieved [12]. It is defined as $\mu_s = 100 \times \mu_p$ in our CFD model.

In the study, values of critical shear rate were taken from study of Susan-Resiga [14] that carried out in range of 0.1 A to 3 A for MRF-132DG fluid. $\dot{\gamma}_k$ is 0.001 s⁻¹ and 0.002 s⁻¹ for 1 A and 1.5 A, respectively. 0.0015 s⁻¹ is calculated by interpolation for 1.25 A. Susan-Resiga [14] proposed to use a function as $\tan h(\dot{\gamma}/\dot{\gamma}_k)$, $erf(\dot{\gamma}/\dot{\gamma}_k)$ or $1 - e^{-(\dot{\gamma}/\dot{\gamma}_k)}$ in order to avoid the discontinuity in the flow curve in transition from Newtonian region to non-Newtonian region. In the CFD model of the study, yield stress that can be provided the continuity was calculated as follows by using a tan h function considering the critical point, $\dot{\gamma}_k$.

$$\tau_{y,k} = \tau_y \tan h \frac{\dot{\gamma}}{\dot{\gamma}_k} \quad (37)$$

Piston is moved as sinusoidal into cylinder. The sinusoidal movement and velocity are defined with the following equations:

$$S = S_{max} \cos(\omega t_s) \quad (38)$$

$$u_p = u_{max} \sin(\omega t_s) \quad (39)$$

where t_s is timestep, ω is angular velocity, S_{max} and u_{max} are maximum stroke and maximum velocity, respectively. Analyses have been realized for each timestep until to reach total time of a cycle of piston. In the study, timestep, maximum stroke and

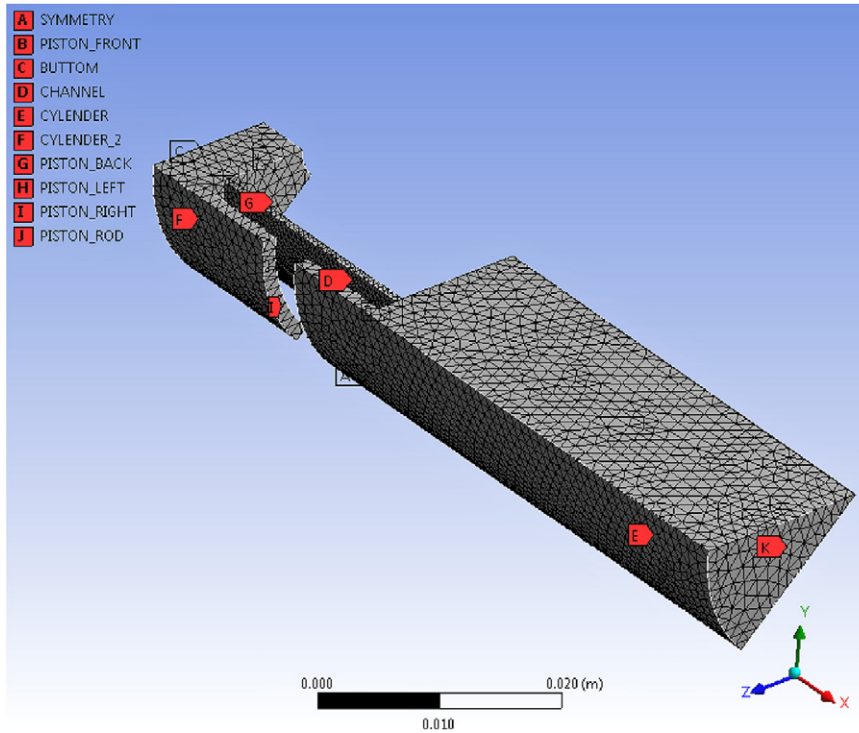


Fig. 5. Mesh and boundaries of computational domain.

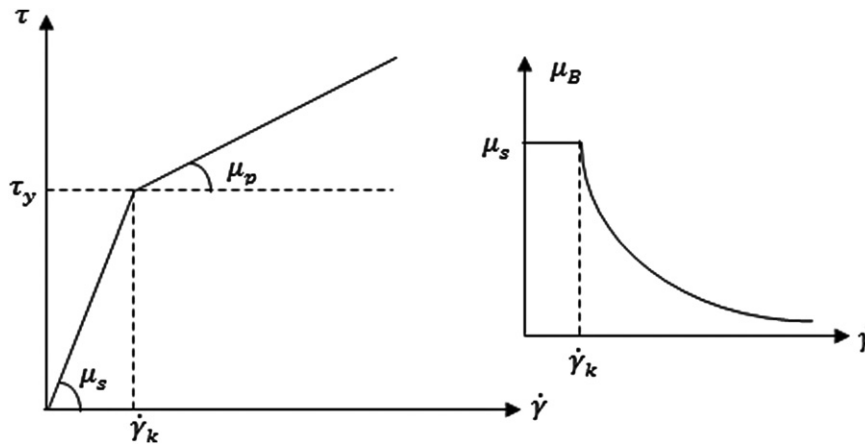


Fig. 6. Bingham CFD model.

maximum velocity were specified in parallel to experimental studies as 0.01 s, 0.015 m, and 0.05 m/s, respectively.

The CFX code solves Navier–Stokes equations using a finite volume method for the equation discretization. Heat transfer in a fluid domain is governed by the thermal energy equation on CFX (Eq. (40)).

$$\frac{\partial(\rho h)}{\partial t} - \frac{\partial p}{\partial t} + \nabla(\rho \mathbf{U}h) = \nabla(\lambda \nabla T) + \mathbf{U} \nabla p + \tau : \nabla \mathbf{U} + S_E \quad (40)$$

The term $\tau : \nabla \mathbf{U}$ is always positive and called viscous dissipation and τ is the molecular stress tensor (including both normal and shear components of the stress) [23].

A second-order high resolution approximation was used for the advection terms. Convergence criteria and coefficient loop were specified as 1.10^{-4} and 10, respectively.

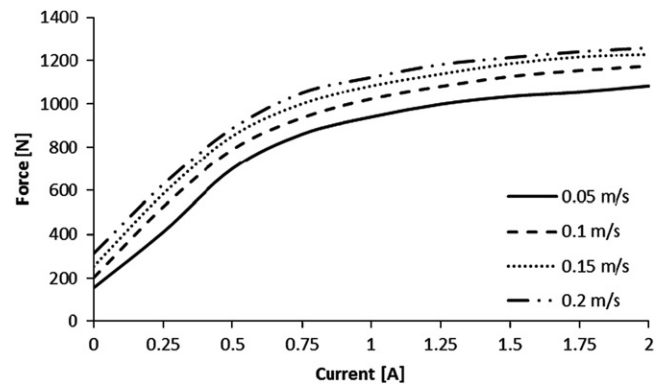


Fig. 7. Damper force vs. current excitation varying with piston velocity at stroke=25 for damper 1.

5. Test results and validation of the proposed model

5.1. Test results

MR dampers were tested at current of 0 A, 0.25 A, 0.5 A, 0.75 A, 1 A, 1.5 A, 1.75 A and 2 A. Curves of maximum damper forces vs. currents at changing values of piston velocity can be seen in Figs. 7–9 and at changing values of stroke can be seen in Figs. 10–12.

As can be seen in Figs. 7–12, damper force varies exponentially with the applied current. Damper force especially increases linearly up to 1A, however, this increase decays gradually at higher excitation currents, i.e., 1.0–2.0 A, which can be attributed

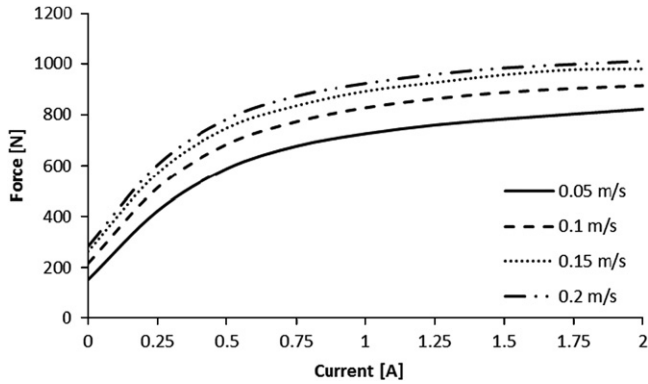


Fig. 8. Damper force vs. current excitation varying with piston velocity at stroke=25 for damper 2.

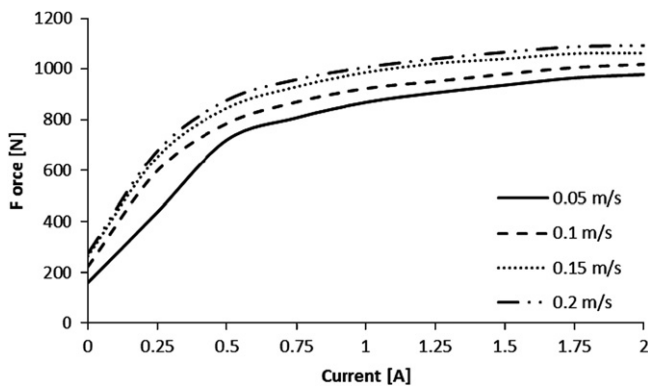


Fig. 9. Damper force vs. current excitation varying with piston velocity at stroke=25 for damper 3.

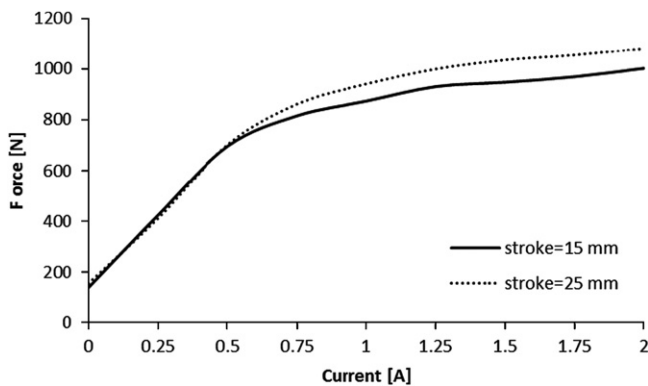


Fig. 10. Damper force vs. current excitation varying with stroke at piston velocity=0.05 m/s for damper 1.

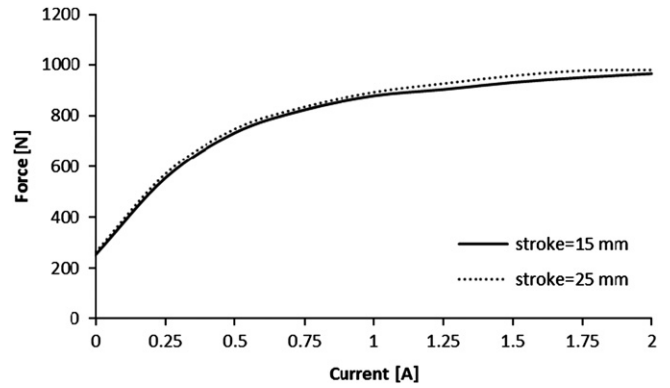


Fig. 11. Damper force vs. current excitation varying with stroke at piston velocity=0.15 m/s for damper 2.

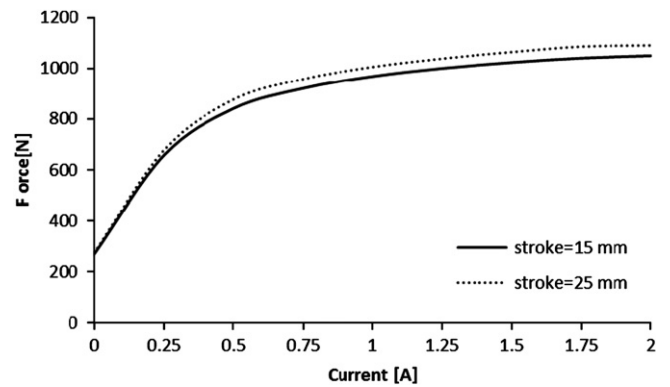


Fig. 12. Damper force vs. current excitation varying with stroke at piston velocity=0.2 m/s for damper 3.

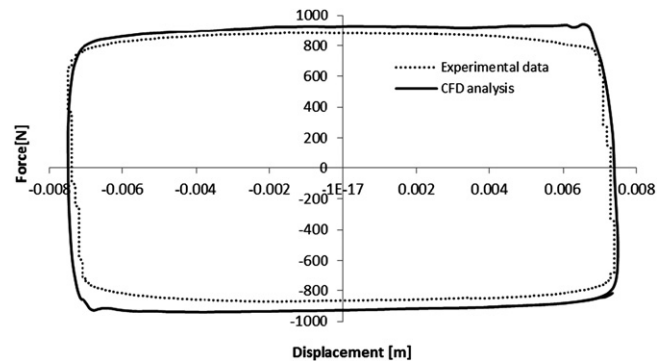


Fig. 13. Damper force vs. displacement for damper 1.

to the fact that MR damper is magnetically saturated with increasing excitation current. In short, damper force does not increase remarkably in current values much larger than 1 A.

Tests of MR dampers were performed for 0.05 m/s, 0.1 m/s, 0.15 m/s and 0.2 m/s of piston velocity. Results of the test exhibit that damper forces in 0.15 m/s and 0.2 m/s of piston velocity are very close each other (see Figs. 7–9). It is pointed that the rate of rise of damper force decreases substantially in larger than 0.15 m/s of piston velocity.

Values of damper force were investigated under magnetic field, up to 2 A, in 15 mm and 25 mm stroke when piston velocity was kept constant. One can observe from Figs. 10–12 that up to 0.5 A, damper forces nearly equal each other for 15 mm and 25 mm of stroke. while increasing the current value, the damper force is separated from each other and larger stroke values gives larger damper force.

5.2. Validation of the CFD analysis

In this section the CFD analysis model has been verified by comparing the model results with the experimental data. The comparisons are presented in Figs. 13–15 as curves of damper force vs. displacement. It is observed that the predicted values by CFD model agree well with the measured values. Nevertheless, because deformed mesh brings with it some handicaps, the agreement didn't accrue in desired level. It can be especially seen at ends of stroke where piston reaches to upper and bottom dead points at which direction of flow changes. In addition, in order to minimize dependence of mesh on solution and to get better solution, very different mesh structures should be carried out with the same analysis so that dependence of mesh on the solutions can be determined.

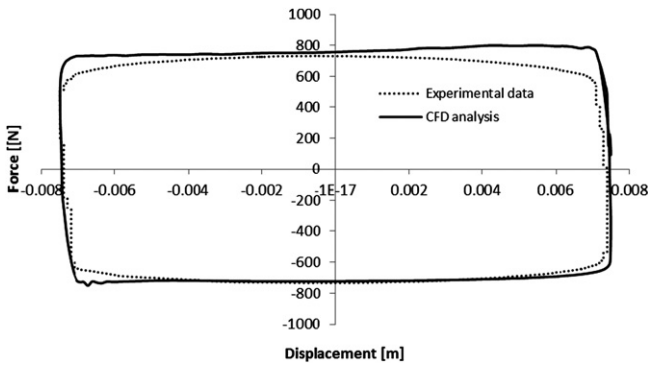


Fig. 14. Damper force vs. displacement for damper 2.

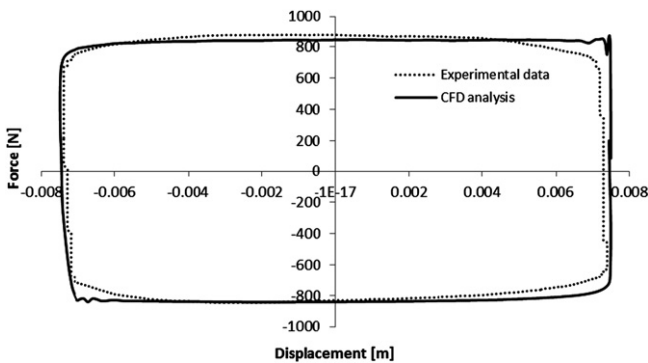


Fig. 15. Damper force vs. displacement for damper 3.

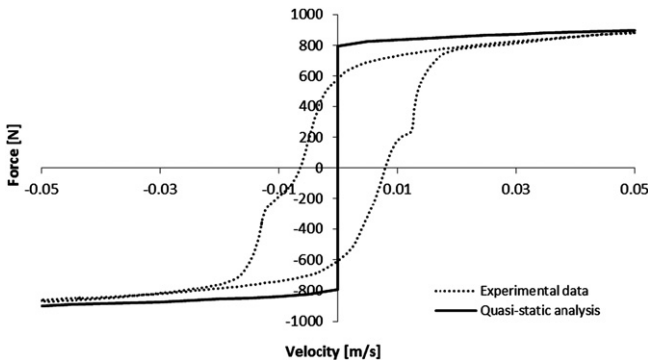


Fig. 16. Damper force vs. piston velocity for damper 1.

5.3. Validation of the quasi-static analysis

Nonlinear equation system consisting of Eqs. (23) and (25), which has two unknowns r_a and r_b , which determine the plug thickness, has been solved by the Newton–Raphson method by using the MATLAB code. After the calculation to be determined the plug thickness, pressure drop through the annular gap and damper force can be obtained. Once the equation system had been solved at certain range of piston velocity up to its maximum value, damper force can be determined for different piston velocity, thus quasi-static analysis model has been verified by comparing the model results with the experimental data. The comparisons are presented in Figs. 16–18 as curves of damper force vs. piston velocity. It is observed that the predicted values by the quasi-static model agree with the measured values, except in the hysteretic region seen in the curve of force vs. velocity. The quasi-static flow models can be successfully adapted to design MR dampers, they unfortunately fail to capture the dynamic operational behavior of these dampers [17]. Nevertheless, the model can be successfully adopted to predict the dynamic operating range of MR dampers.

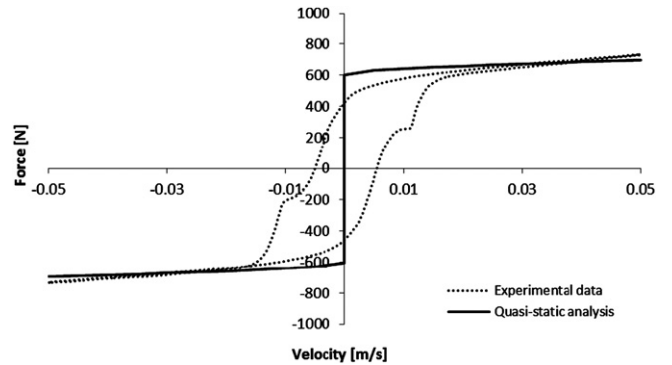


Fig. 17. Damper force vs. piston velocity for damper 2.

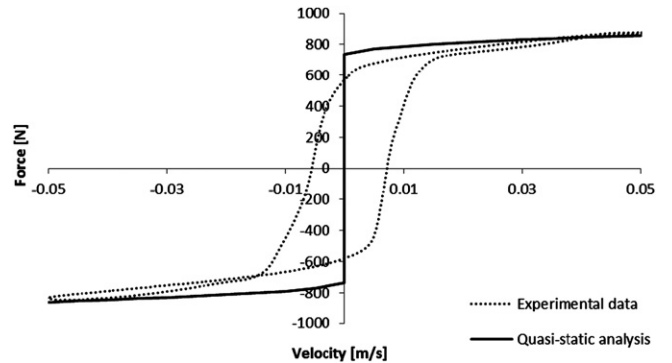


Fig. 18. Damper force vs. piston velocity for damper 3.

Table 3
Pressure gradients and plug region thicknesses calculated by Eq. (10).

Damper no.	dp/dz (kg/m ² s ²)	$\delta_{analytical}$ (mm)
1	-122,755,010.2	0.5287
2	-112,538,815	0.5288
3	-102,686,265.3	0.5277

5.4. Comparisons of plug region thickness

Plug region thickness in Eq. (10) and pressure drop in Eq. (28) are a function of pressure gradient. In order to calculate plug region thickness from Eq. (10), pressure gradient should be known. Pressure gradient is calculated from Eq. (28) at value of pressure drop that is obtained from Eq. (29). The pressure gradients and plug region thicknesses ($\delta_{analytical}$) can be seen in Table 3.

Nondimensional plug region thickness can be calculated by Eq. (33) depending on the nondimensional Bingham number, then plug region thickness is obtained by Eq. (34). The results of the calculation can be seen in Table 4.

Plug region thicknesses can be also calculated by obtaining r_a , starting location of plug region, and r_b , ending location of plug region, by solving numerically of Eqs. (23) and (25). In Table 5 can be seen values r_a and r_b and plug region thicknesses.

According to comparison of the these three calculations to be done among each other exhibit that largest deviation is 5.23% and mean deviation is 1.81%.

The velocity profiles can be seen in Fig. 19, which were obtained by solving numerically of Eqs. (23) and (25) to calculate plug region thicknesses then velocity profiles specified Eqs. (14) and (18), occurred in gap consisting of I, II and III regions. As can be seen in Fig. 19, for a damper configuration, velocity profiles in the annular gap that is under magnetic field are calculated. It is observed while increasing current, plug velocity increases. But, rising tendency declines by increasing current, the situation can

Table 4
Bi numbers and plug region thicknesses calculated by Eq. (34).

Damper no.	Bi	δ_{Bi} (mm)
1	248.22	0.5269
2	227.62	0.5240
3	207.28	0.5206

Table 5
 r_a and r_b and plug region thicknesses obtained by Eqs. (23) and (25).

Damper no.	r_a (mm)	r_b (mm)	$\delta_{numerical}$ (mm)
1	11.937	12.461	0.5245
2	11.945	12.453	0.5085
3	11.945	12.453	0.5085

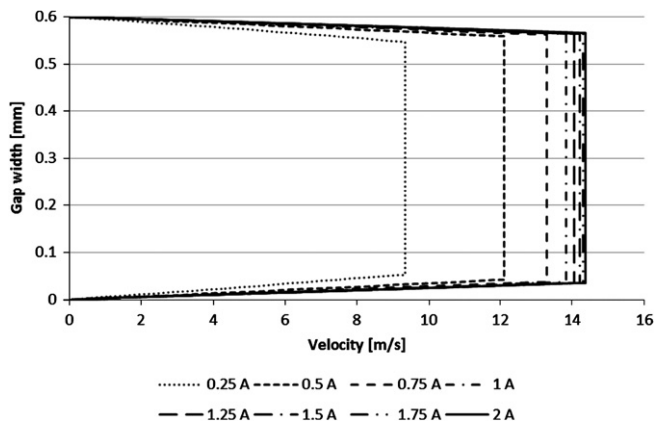


Fig. 19. Velocity profiles depending on current excitations for damper 1 at 0.05 m/s of piston velocity.

be explained with saturation of the damper. The saturation obviously can be seen after 1A.

6. Conclusions

One of the purposes of the study was to examine effect of piston velocity and stroke of MR damper on the damper performance. In addition, CFD analysis were performed with transient and deformed mesh to simulate movement of piston head in the damper considering non-Newtonian regions in the annular gap due to exposed magnetic field on the MR fluid. On the other hand, a quasi-static model was proposed to calculate damper force and specified plug thickness in the annular gap. Three MR dampers were manufactured and tested to confirm the quasi-static and CFD model in the study.

A series of tests was conducted for each MR damper to obtain the dynamic response of the damper by varying the applied current from 0 to 2 A in increments of 0.25 A, while maintaining the piston velocity and stroke at constant levels. The tests were carried out at velocity of 0.05 m/s, 0.1 m/s, 0.15 m/s and 0.2 m/s and at stroke of 15 mm and 25 mm. Results showed that damper force especially increases linearly up to 1 A, however, this rising decays gradually at higher currents between 1 A and 2 A due to saturation. In addition that damper force was very close each other in 0.15 m/s and 0.2 m/s of piston velocity. It was observed that the rate of increase of damper force decreases substantially in larger than 0.15 m/s of piston velocity. Up to 0.5 A, damper forces were occurred at very close values for 15 mm and 25 mm of stroke, while increasing the applied current, test performed at larger stroke provided bigger damper force.

Thanks to the CFD analysis that performed with deformed (moving) mesh and transient, rebound and compression movement of piston could be modeled in real work principle of the damper. Moreover, flow magnitudes (flow velocity, pressure, dynamic viscosity, temperature shear rate etc.) in any position of the piston could be obtained easily. In the CFD analysis, the Bingham plastic model was employed to model the non-Newtonian region, which is exposed to magnetic field, in the gap. Value of yield stress in Bingham plastic model varying to current excitation was obtained from magnetic flux density by converting to yield stress using the equation that gives relationship between magnetic flux density and yield stress. Also, be able to catch up non-Newtonian regions in the gap for any time in moving mesh, CCL expressions were written in ANSYS CFX. CFD analyses were performed for three dampers specified and the results of these analyses were compared to experimental data. A good agreement for curves of damper force–displacement has been observed between the experimental and simulated data. Nevertheless, because of handicaps of deformed mesh, the agreement has not got in desired levels.

In the study a quasi-static model based on Navier–Stokes equations was proposed by assuming that regions exposed magnetic field behave in accordance with Bingham plastic model. Pressure drop through the annular gap was obtained in terms of MR fluid properties, MR damper geometry and volume flow rate. Pressure gradient is a key parameter to get plug thickness that characterizes non-Newtonian flow in the annular gap. Radius of starting and end point of the plug region in reference to centerline of the damper, which are two unknowns in the nonlinear equation system that enabled to solve by the Newton–Raphson method using the MATLAB code, could be calculated to determine the plug thickness. Thus, pressure drop through the annular gap and damper force could be obtained. Once the equation system had been solved at certain range of piston velocity up to its maximum value, curves of damper force–piston velocity could be

plotted. The results were compared to experimental ones and a good agreement was seen excepting hysteresis behaviors that arise from inherent of quasi-static analysis.

Plug thicknesses obtained from the quasi-static analysis presented in the study were compared to ones calculated from Wereley and Pang [1] model depended to dimensional Bi number and an analytical method presented firstly in the study. The results showed that mean deviation among the calculations became as 1.81%. Also, the quasi-static model and the analytical method will be able to used to calculate the plug thickness in future. In addition, velocity profiles in the annular gap were depicted for various currents, it was observed that plug thickness and velocity increased by increasing of current. Rate of the rising decreased together with increasing of current especially bigger than 1 A due to saturation.

Acknowledgment

The authors gratefully acknowledge TUBITAK for making this project possible under Grant no:104M157.

References

- [1] Wereley NM, Pang L. Non-dimensional analysis of semi-active electrorheological and magnetorheological dampers using approximate parallel plate models. *Smart Mater Struct* 1998;5(7):732–43.
- [2] Felt DW, Hagenbuchle M, Liu J, Richard J. Rheology of a magnetorheological fluid. *J Intell Mater Syst Struct* 1996;5(7):589–93.
- [3] Dimock GA, Lindler JE, Wereley NM. Bingham biplastic analysis of shear thinning and thickening in magnetorheological dampers. *Smart Struct Mater* 2000;3985:444–55.
- [4] Hesselbach H, Abel-Keilhack C. Finite element flow analysis of magnetic fluids with yield stress. *Book of Abstracts des 5. Mülheim/Ruhr: Deutschen Ferrofluid-Workshop*; 2003 15–6.
- [5] Wang X. Nonlinear behavior of magnetorheological (MR) fluids and MR dampers for vibration control of structural systems, PhD thesis. Reno: University of Nevada; 2002.
- [6] Wang X, Gordaninejad F. Flow analysis and modeling of field-controllable electro- and magneto-rheological fluids dampers. *J Appl Mech* 2007;74(1): 13–22.
- [7] Yasrebi N, Ghazavi A, Mashhadi MM. Magneto-rheological fluid dampers modeling: numerical and experimental. In: *Proceedings of the 17th IASTED international conference modeling and simulation*; 2006.
- [8] Widjaja J, Samali B, Li J. Electrorheological and magnetorheological duct flow in shear-flow mode using Herschel–Bulkley constitutive model. *J Eng Mech* 2003;129(12):1459–65.
- [9] Ericksen EO, Gordaninejad F. A magneto-rheological fluid shock absorber for an off-road motorcycle. *Int J Veh Des* 2003;33:138–52.
- [10] Attia HA, Ahmed MES. Circular pipe MHD flow of a dusty bingham fluid. *Tamkang J Sci Eng* 2005;8(4):257–65.
- [11] Li WH, Du H. Design and experimental evaluation of a magnetorheological brake. *Int J Manuf Technol* 2003;21:508–15.
- [12] Bullough WA, Elam DJ, Wong AP, Tozer RC. Computational fluid dynamics in the flow of ERF/MRF in control devices and of oil through piezo-hydraulic valves. *Comput Struct* 2008;86(3–5):266–80.
- [13] Ellam DJ, Atkin RJ, Bullough WA. Analysis of a smart clutch with cooling flow using two-dimensional Bingham plastic analysis and computational fluid dynamics. *Proc ImechE: Power Energy* 2005;219(8):639–52.
- [14] Susan-Resiga D. A Rheological model for magneto-rheological fluids. *J Intell Mater Syst Struct* 2009;20(8):1001–10.
- [15] Lelic U, Kok WBJ. Heat flows in piston compressors. In: *Proceedings of the 5th European thermal-sciences conference. The Netherlands*; 2008.
- [16] Bompos DA, Nikolakopoulos PG. CFD simulation of magnetorheological fluid journal bearings. *Simulation Model Pract Theory* 2010;19(4):1035–60.
- [17] Çeşmeci Ş, Engin T. Modeling and testing of a field-controllable magnetorheological fluid damper. *Int J Mech Sci* 2010;52(8):1036–46.
- [18] Rosenfeld NC, Wereley NM. Volume-constrained optimization of magnetorheological and electrorheological valves and dampers. *Smart Mater Struct* 2004;13:1303–13.
- [19] Nguyen QH, Han YM, Choi SB, Wereley NM. Geometry optimization of MR valves constrained in a specific volume using the finite element method. *Smart Mater Struct* 2007;16(6):2242–52.
- [20] Nguyen QH, Choi SB. Dynamic modeling of an electrorheological damper considering the unsteady behavior of electrorheological fluid flow. *Smart Mater Struct* 2009;18(5):055016 8pp.
- [21] Ghita G, Giuclea M, Sireteanu T. Modeling of dynamic behavior of magnetorheological fluid damper by genetic algorithms based inverse method. In: *Proceedings of the 6th international conference on hydraulic machinery and hydrodynamics*; 2004. p. 21–2.
- [22] Spencer BF, Yang G, Carlson JD, Sain MK. Smart dampers for seismic protection of structures: a full-scale study. In: *Proceedings of the second world conference on structural control*; 1998.
- [23] ANSYS, Solver Theory Guide, ANSYS CFX Release 12.1 Manual, 2010.